IFNγ expression correlates with enhanced cytotoxicity in CD8^{+} T cells

Varsha Pattu[2#], Elmar Kause[2], Hsin-Fang Chang[2], Jens Rettig[2], Xuemei Li[1,2*#]

[1] Department of Neurology, NHC Key Laboratory of Diagnosis and Treatment on Brain Functional Diseases, The First Affiliated Hospital of Chongqing Medical University, No.1 Youyi Road, Yuzhong District, Chongqing, 400016, China

[2] Cellular Neurophysiology, Center for Integrative Physiology and Molecular Medicine, (CIPMM), Saarland University, 66421 Homburg, Germany

[#] These authors contributed equally to this work and share first authorship

* Correspondence: 860941986@qq.com

Abstrat

Background: CD8+ T lymphocytes (CTLs) act as serial killers of infected or malignant cells by releasing large amounts of interferon-gamma (IFNγ) and granzymes. Although IFNγ is a pleiotropic cytokine with diverse immunomodulatory functions, its precise spatiotemporal regulation and role in CTL-mediated cytotoxicity remain incompletely characterized.

Methods: Using wild-type (WT) and granzyme B-mTFP knock-in mice, we combined in vitro approaches, including T-cell isolation and culture, plate-bound anti-CD3e stimulation, degranulation assays, flow cytometry, immunofluorescence, and structured illumination microscopy, to investigate IFNγ dynamics in CTLs.

Results: IFNγ expression in CTLs was rapid, transient, and strictly dependent on T-cell receptor (TCR) activation. We identified two functionally distinct IFNγ-producing subsets: IFNγ^{high} (IFNγ^{hi}) and IFNγ^{low} (IFNγ^{lo}) CTLs. IFNγ^{hi} CTLs exhibited an effector/effector memory phenotype, significantly elevated CD107a surface expression (a marker of lytic granule exocytosis), and pronounced colocalization with cis-Golgi and granzyme B compared to IFNγ^{lo} CTLs. Furthermore, CRTAM, an early activation marker, correlated with IFNγ expression in naive CTLs.

Conclusion: Our findings establish a link between elevated IFNγ production and enhanced CTL cytotoxicity, implicating CRTAM as a potential regulator of early CTL activation and IFNγ induction. These insights provide a foundation for optimizing T cell-based immunotherapies against infections and cancers.

Keywords: CD8+ T cells, interferon-gamma, CD107a, cytotoxicity, subcellular localization, CRTAM

Introduction

$CD8^+$ cytotoxic T lymphocytes (CTLs) are critical immune sentinels that protect the host against infections and malignancies. Upon antigen recognition by specialized antigen-presenting cells (APCs), naive $CD8^+$ T cells (T_N) undergo clonal expansion and differentiate into short-lived effector CTLs (T_E), which migrate to peripheral tissues and inflammatory sites[1,2]. Most T_E undergo apoptosis during the contraction phase[3], while a small subset persists as long-lived memory T cells (T_M). These memory populations consist of at least two distinct subsets: central memory (T_{CM}) and effector memory (T_{EM}) T cells[4,5]. In mice, short-lived T_E downregulate L-selectin (CD62L) but retain partial expression of IL-7 receptor alpha (CD127)[6], whereas long-lived T_M constitutively express CD127. T_{CM} exhibit high CD62L expression, while T_{EM} downregulate CD62L. Notably, under chronic infections or cancer, persistent antigen exposure can drive naive T cells into a dysfunctional state termed T cell exhaustion (T_{EX})[7]. Understanding the heterogeneity and function of CTL substets is crucial to discern the complex dynamics of immune responses in various disease[8].

CTLs eliminate target cells through lytic (granzymes and perforin) and non-lytic (IFNγ and TNFα) mechanisms[9,10]. Their effector functions are regulated by transcription factors such as T-bet, Eomes, CRTAM (Class-I MHC-restricted T-cell associated molecule), T-box, and Runx family proteins[11–13]. The killing capacity of CTLs depends on cytotoxic granules (CGs) and degranulation efficiency[14]. CGs are secretory lysosomes (SGs) containing granzymes and perforin[15], enclosed by a lipid bilayer embedded with lysosome-associated membrane glycoproteins (LAMPs), including CD107a (LAMP-1), CD107b (LAMP-2), and CD63 (LAMP-3)[16]. Upon target recognition, CGs fuse with the plasma membrane, releasing their cytotoxic substances via exocytosis[13]. Since resting CTLs lack surface LAMPs, CD107a/b expression serves as a quantitative marker for degranulation[12]. Additionally, Fas ligand (FasL/CD95L), stored in specialized SGs, is externalized during degranulation to induce apoptosis in target cells[17]. Intriguingly, CTLs also express Fas receptor (Fas), enabling fratricidal killing (CTL-fratricide)—a mechanism that

eliminates effector T cells during immune contraction[17].

Beyond direct cytotoxicity, CTLs exert effector functions via interferon-gamma (IFNγ) and tumor necrosis factor-alpha (TNFα) secretion. IFNγ is primarily produced by NK cells, Th1 cells, and $CD8^+$ T cells[18,19]. In murine models of *Mycobacterium tuberculosis* infection, $CD4^+$ and $CD8^+$ T cells are the dominant IFNγ producers in vivo[20]. IFNγ is a pleiotropic cytokine with dual roles—exhibiting antiviral[21,22] and antitumor activity while paradoxically promoting tumor progression in certain contexts[23–25]. Mechanistically, IFNγ signaling upregulates interferon regulatory factor-1 (IRF-1), which enhances MHC-I/II expression, rendering target cells more susceptible to CTL attack[26]. As a proinflammatory cytokine, IFNγ also activates macrophages to secrete TNFα and IL-6[27–29].

In this study, we investigated IFNγ production, subcellular localization, cellular subtypes, and cytotoxic function in IFNγ-expressing CTLs. We found that naive $CD8^+$ T cells rapidly acquire IFNγ production within 2 hours of TCR activation whereas GzmB expression is restricted to effector CTLs with mature immune synapses[30]. Activated CTLs exhibited transient, TCR-dependent IFNγ expression, contrasting with pre-stored GzmB in resting CTLs. Strikingly, $IFN\gamma^+$CTLs segregated into $IFN\gamma^{hi}$ and $IFN\gamma^{lo}$ subsets, while $GzmB^+$CTLs were homogeneous. $IFN\gamma^{hi}$ cells displayed a T_E/T_{EM} phenotype (low CD62L), whereas $IFN\gamma^{lo}$ cells resembled T_{CM} (high CD62L). Degranulation assays revealed that $IFN\gamma^{hi}$ CTLs exhibited significantly higher surface CD107a than $IFN\gamma^{lo}$ cells, suggesting superior lytic activity. Furthermore, $IFN\gamma^{hi}$ CTLs showed pronounced colocalization with cis-Golgi and $GzmB^+$ vesicles, reinforcing the link between IFNγ expression and cytotoxicity. Finally, comparative analysis of IFNγ and CRTAM expression in naive vs. activated $CD8^+$ T cells suggested that CRTAM may regulate early T cell activation and IFNγ production.

Methods

Mice

Wild-type (WT) mice were purchased from Charles River， and granzyme B-mTFP knock-in (GzmB-mTFP KI) mice were generated as previously described[30]. All experimental procedures were conducted in compliance with regulations of the state of Saarland (Landesamt für Verbraucherschutz, AZ.: 2.4.1.1 and 11/2021).

Cell isolation

Mice were anesthetized with CO_2 and executed by cervical dislocation. The left abdominal cavity was exposed, and the spleen was carefully removed, placed on a 70 μm cell strainer (Corning Life Sciences) and ground. The grinding slurry remaining on the strainer was rinsed with RPMI medium, and the cell suspension (10 mL) was collected into a 15 mL sterile centrifuge tube (Corning Life Sciences) and centrifuged (6 min, 1100 rpm without a break) to wash the splenocytes. Washed splenocytes were mixed and incubated with erythrocyte lysis buffer (1 mL) for 30 seconds to lyse the erythrocytes therein. Immediately, 10 mL of ice-cold RPMI was added to terminate lysis and centrifuged (6 min, 1100 rpm), and the cell sediment was washed once more with isolation buffer to remove erythrocyte debris. Primary $CD8^+$ T lymphocytes were positively isolated from spleens according to the instructions of the Dynabeads FlowComp Mouse CD8 Kit (Thermo Scientific).

Cell culture

Isolated primary $CD8^+$ T lymphocytes were cultured at a density of 1×10^6 cells/mL in AIM V medium (Gibco) supplemented with 10% FCS, 50 μM β-Mercaptoethanol (BME), and 100 U/mL recombinant mouse

113 IL-2 (Life technology) and stimulated with anti-CD3e/anti-CD28 magnetic beads (number of cells: magnetic
114 beads = 1:0.8, Thermo Fisher Scientific) to generate activated CTLs. Cells were cultured in 24-well plates in
115 a cell culture incubator (37 °C, 5% CO_2, saturated humidity) according to the protocol of Bzeih et al.
116 (2016)[41]. The first passaging of the cells was started after 2 days of culture and then once a day with the
117 addition of fresh AIM V medium supplemented with 10% FCS, 50 µM BME and 100 U/mL recombinant
118 IL-2. Usually, day3 to day5 cells were used for experiments.

119 For some experiments, cells were used immediately after the CD3e/CD28 activation beads had been
120 removed. For most experiments cells were allowed to recover for 2 h after CD28/CD3e beads had been
121 removed. Those cells underwent a "re-stimulation" during the experiment. By this is meant that by
122 appropriate measures, the T-lymphocyte receptors have been acutely stimulated to trigger cytotoxic actions,
123 such as the release of GzmB and IFNγ. For FACS experiments: To induce intracellular IFNγ-expression,
124 day3-5 beads-activated WT CTLs were washed and restimulated with optimal concentration of plate-bound
125 anti-CD3e antibody (10 µg/mL) from Estl et al. (2020)[29] for 0, 0.5 h, 1 h, 2 h, 3 h, and 4 h, 6 h, 8 h, 12 h and
126 24 h in a cell culture incubator.

127

128 **Immunocytochemistry**

129 CTLs were stained with an anti-IFNγ antibody to detect endogenous IFNγ. Therefore, cells were fixed with
130 freshly prepared ice-cold 4% paraformaldehyde in DPBS (1×) and washed in DPBS (1×) containing 0.1 M
131 glycine (quenching of autofluorescence). After a second wash cells were permeabilized with for 20 minutes
132 in DPBS (1×) containing 0.1% Triton-X 100 (Roth), then blocked for 20-30 minutes in blocking buffer
133 contained 5% BSA. Finally, cells were stained with primary rat anti-mouse IFNγ (1:200) and secondary
134 anti-rat antibodies (1:1000), or rat anti-mouse IFNγ-Alexa488 (1:200), before they were mounted and

135 imaged using high-resolution structured illumination microscopy (SIM).

136 Antinodies used in this study were listed in Extended Data Table1.

137

138 Structure illumination microscopy

139 Structured illumination microscopy setup

140 The SIM setup was from Zeiss (ELYRA PS.1). Images were acquired using a 63× Plan-Apochromat (NA1.4)
141 objective with excitation light of 488, 561, and 647 nm and then processed for SIM to obtain higher
142 resolutions. Z-stacks of 200 nm step size were used to scan cells. Zen 2012 software (Zen 2012; Carl Zeiss)
143 was used for the acquisition and processing of the images for higher resolutions.

144 Colocalization analysis

145 For colocalization analysis the JACoP plugin (Bolte 2006) of Fiji (Johannes, 2012) was used. Pearson's and
146 Manders' overlap coefficients (Manders et al., 1993) were used for quantification of the degree of
147 colocalization.

148

149 Flow cytometry

150 Intracellular IFNγ measurement

151 WT CTLs were washed with DPBS (1×) after restimulation for 0.5 h, 1 h, 2 h, 3 h, 4 h, 6 h, 8 h, 12 h, and 24
152 h with plate-bound anti-CD3e antibody (10 μg/mL). The pellet (0.5 × 10^6 CTLs) was resuspended in 250 μL
153 fixation buffer and incubated on ice for 10 min using BD Cytofix/ Cytoperm™ Fixation/Permeabilization Kit
154 (554714, BD Bioscience). Next, CTLs were centrifuged, resuspended in 100 μL wash buffer (1×) and stained
155 for intracellular IFNγ and GzmB with rat anti-mouse IFNγ-Alexa488 (1:200) and rat anti-mouse
156 GzmB-Alexa647 (1:200)) on ice (1 h). Cells were washed and measured by flow cytometry (FACS, BD

157 FACSAria III). Data were analyzed using FlowJo v10.10.0_CL software (Celeza-Switzerland).

158 **Surface markers analysis**

159 $CD8^+$ T-lymphocytes either with or without (re)stimulation, were taken from cell culture and washed with
160 cold-DPBS (1×). Next they were stained for CD62L, CD69 and CD25 using corresponding fluorescent Abs
161 without fixation (live staining, 30 min on ice). Next, cells were washed twice with cold-wash buffer (1×) and
162 resuspended in cold-DPBS (1×) for FACS analysis.

163

164 **Degranulation assay**

165 Activated WT CTLs were washed and resuspended in AIM V after removing beads from the culture. Cells
166 (0.2×10^6/200 μL) were then cultured on a 10 μg/mL anti-CD3e coated or DPBS (1×) coated 96-well plate
167 with 1 μL anti-CD107a-PE for 3 h at 37 °C for degranulation. The control cells were incubated without
168 anti-CD107a-PE as a background signal. All cells were then washed twice with cold DPBS (1×) and checked
169 by FACS. Data were analyzed using FlowJo software. Gates were set according to no fluorescence control
170 cells. Each independent experiment had a duplicate.

171

172 **Statistical analysis**

173 For data analysis and to calculate the statistical significance, Fiji, ImageJ-win64, Microsoft Excel
174 (Microsoft), SigmaPlot 13 and GraphPad_Prism10.2.3 were used. The respective method to calculate
175 statistical significance was given in the text for each figure. Figures were generated using
176 FlowJo_v10.10.0_CL, GraphPad_Prism, Excel and PowerPoint.

177

178 # Results

179 ## Transient IFNγ expression depends on TCR re-activation in resting CTLs

180 To determine whether interferon-gamma (IFNγ) expression is constitutive or regulated in activated CTLs, we
181 analyzed intracellular IFNγ dynamics following TCR re-stimulation as previous report[31]. Day 3–5 activated
182 CTLs, with or without re-stimulation, were fixed, permeabilized (BD Cytofix/Cytoperm™), and stained for
183 IFNγ-Alexa488 and GzmB-Alexa647 (without Golgi transport inhibition). Flow cytometry data were
184 acquired and analyzed using FlowJo v10.

185 IFNγ- and GzmB- expressing CTLs was shown in pseudocolor plots in 4 h TCR re-stimulation (Figure
186 1A,B). In unstimulated CTLs, IFNγ was nearly undetectable, but its expression increased rapidly upon TCR
187 re-stimulation (Figure 1A). Whereas large amount of GzmB exisited before restimulation and had less
188 variation after TCR re-stimulation (Figure 1B). The expression level of IFNγ and GzmB in CTLs exhibited a
189 maturation-dependent pattern and distinct kinetics. IFNγ expression (measured by Median fluorescence
190 intensity, MFI) showed a transient peak (Figure 1C), with day 5 CTLs displaying faster upregulation than
191 day 3 CTLs at 2 h ($p = 0.020$), 3 h ($p = 0.004$), and 4 h ($p = 0.004$). Day 4 CTLs showed IFNγ MFI kinetics
192 comparable to day 5 CTLs but significantly faster than day 3 at 3 h ($p = 0.044$). In contrast, GzmB MFI
193 remained stable across day 3-5 CTLs during the 4-hour restimulation period (Figure 1D).

194 Longitudinal analysis revealed divergent temporal patterns: IFNγ levels peaked at 12 h before declining
195 sharply by 24 h, while GzmB accumulated continuously. IFNγ MFI was significantly elevated at 6 h, 8 h,
196 and 12 h compared to 24 h ($p = 0.021$, $p = 0.017$, and $p = 0.021$, respectively) (Figure 1E). Conversely,
197 GzmB MFI showed progressive accumulation, with significantly higher levels at 24 h versus 4 h, 6 h, and 8
198 h ($p = 0.021$, $p = 0.037$, and $p = 0.039$), and at 12 h versus 4 h ($p = 0.042$) (Figure 1F).

199 In conclusion, in activated CTLs, the expression of IFNγ and GzmB exhibited a maturation-dependent

200 pattern and distinct kinetics. IFNγ expression is transient, but GzmB expression lasts longger compared to
201 IFNγ after TCR (re-)activation.

202

203 CTL subtype dynamics upon TCR re-stimulation

204 Cytotoxic T lymphocytes (CTLs) comprise distinct functional subsets, including effector cells (T_E),
205 effector-memory cells (T_{EM}), and central-memory cells (T_{CM}). To determine whether IFNγ expression is
206 subtype-specific and whether TCR re-stimulation alters the subtype composition of cultured CTLs, we
207 stimulated activated CTLs with 10 μg/mL plate-bound anti-CD3e[31] for 0.5–4 h and analyzed subtype
208 markers ($CD44^{hi}$ for T_E/T_{EM}, $CD62^{hi}$ for T_{CM}) by flow cytometry at multiple timepoints.

209 Neither the percentage of $CD44^+$ cells (Extended Data Figure 1A) nor CD44 MFI (Extended Data Figure 1B)
210 changed significantly during 4 h re-stimulation, regardless of culture day (day 3–5), indicating that overall
211 effector differentiation status of the culture remained stable, independent of TCR re-stimulation or culture
212 duration. In contrast, $CD62L^+$ cell frequency (Extended Data Figure 1C) and CD62L MFI (Extended Data
213 Figure 1D) declined sharply upon re-stimulation ($p < 0.05$), indicating a transition from T_{CM} to T_{EM} (Figure
214 2A–C).

215 Pseudocolor plots in quadrant (Figure 2A) revealed subtype distribution. Cells in Q1 (CD44+CD62-) were
216 $T_{E/EM}$, Q2 (CD44+CD62+) were T_{CM}, Q3 (CD44-CD62+) were $T_{N.}$ Day 5 CTLs exhibited significantly more
217 T_E/T_{EM} than day 3 CTLs at 4 h and day 4 CTLs at 1 h/4 h ($p < 0.05$; Figure 2B). Concurrently, T_{CM} frequency
218 was lower in day 5 vs. day 3/day 4 CTLs at 1 h ($p < 0.05$; Figure 2C), confirming that longer culture
219 promotes $T_{E/EM}$ differentiation upon re-stimulation.

220 Screening of activation markers (CD25, CD44, CD62L, CD69) in day 5 CTLs revealed robustly decreased
221 CD62L and increased CD69 in both cell frequency and MFI (Figure 2D,E) after 2 h re-stimulation, while no

222 significant changes were found in CD44 or CD25, implicating CD62L downregulation and CD69
223 upregulation are robust indicators of TCR-driven T_{CM}-to-T_{EM} transition.

224

225 **Cellular subtype and cytotoxicity analysis of IFNγ^{hi} and IFNγ^{lo} CTLs**

226 To determine whether IFNγ expression correlates with cytotoxic T lymphocyte (CTL) effector function, we
227 analyzed reactivated CTLs, which exhibited distinct clusters of high (IFNγ^{hi}) and low (IFNγ^{lo}) IFNγ
228 expression (Figure 1A and Figure 3A, row 1). Using a fluorescence intensity threshold of 10^3, we classified
229 IFNγ-positive CTLs into IFNγ^{hi} and IFNγ^{lo} subsets (Figure 3A, row 2). Longed re-stimulation led to
230 increased effector T cell (T_E) generation (Figure 2B & 3A row3). IFNγ^{hi} subset generated significantly
231 higher ratio of T_E than IFNγ^{lo} subset at 3 and 4 hours of restimulation (Figure 3B).

232 Although IFNγ^{hi} and IFNγ^{lo} CTLs showed comparable CD44 expression, IFNγ^{hi} CTLs exhibited significantly
233 lower CD62L levels compared to IFNγ^{lo} CTLs (Supplement 2). The proportion of T_{CM} was slightly higher in
234 IFNγ^{lo} CTLs, though not statistically significant (Figure 3C). When assessing IFNγ production kinetics,
235 IFNγ^{hi} CTLs displayed markedly higher IFNγ MFI than IFNγ^{lo} CTLs at 2, 3, and 4 hours post-stimulation
236 (Figure 3D), whereas GzmB MFI did not differ significantly between the two subsets (Figure 3E).

237 Extended TCR stimulation revealed a pronounced divergence in IFNγ fluorescence between IFNγ^{hi} and
238 IFNγ^{lo} CTLs by 24 hours (p = 0.001), while GzmB fluorescence remained comparable (Extended Data
239 Figure 3). In IFNγ^{hi} CTLs, IFNγ fluorescence peaked at 12 hours before declining significantly by 24 hours
240 (vs. 4 h, p = 0.042 and p = 0.0025). In contrast, IFNγ^{lo} CTLs exhibited a gradual increase, peaking at 12
241 hours without subsequent decline, and showed higher fluorescence at 6, 12, and 24 hours than at 4 hours (p =
242 0.0483, p = 0.0112, and p = 0.0063, Extended Data Figure 3A). GzmB fluorescence in IFNγ^{hi} CTLs rose
243 significantly at 6, 8, and 24 hours (vs. 4 h, p = 0.0022, p = 0.0075, and p = 0.0213), whereas in IFNγ^{lo} CTLs

244 showed increased GzmB only at 12 and 24 hours (vs. 4 h, $p = 0.0246$ and $p = 0.0171$, Extended Data Figure
245 3B).

246 To evaluate cytotoxic capacity, we measured CD107a surface expression, a marker of degranulation.
247 Unstimulated CTLs exhibited minimal CD107a expression (~5%), but upon 3-hour re-stimulation, levels
248 surged to 21.33% (day 3) and 57% (day 5), with day 5 showing significantly higher degranulation than day 3
249 ($p = 0.0109$; Figure 3F), suggesting that degranulation capacity escalates with CTL maturation. Notably,
250 IFNγ^{hi} CTLs consistently displayed higher CD107a expression than IFNγ^{lo} CTLs (Figure 3G). Flow
251 cytometry histograms depicted CD107a fluorescence intensity in unlabeled (gray), IFNγ^{hi} (pink), and IFNγ^{lo}
252 (blue) CTLs (Figures 3Gi and 3Giii). On day 3, 33.75% of IFNγ^{hi} CTLs underwent degranulation versus only
253 3.76% of IFNγ^{lo} CTLs (Figure 3Gii). By day 5, degranulation frequencies rose to 75.47% (IFNγ^{hi}) and
254 31.13% (IFNγ^{lo}) (Figure 3Giv). These results suggests that cytotoxic activity correlates positively with IFNγ
255 expression and cellular maturation, underscoring the functional superiority of IFNγ^{hi} CTLs.

256

257 **Subcellular localization analysis of IFNγ in IFNγ^{hi} and IFNγ^{lo} CTLs**

258 To characterize the spatial distribution of IFNγ in cytotoxic T lymphocytes (CTLs), we analyzed the
259 Pearson's correlation coefficient (PCC) between endogenous IFNγ, cis-Golgi, and granzyme B (GzmB) in
260 IFNγ^{hi} and IFNγ^{lo} subsets.

261 *IFNγ colocalized with the Golgi Apparatus.* Wild-type (WT) CTLs were re-stimulated with plate-bound
262 aCD3e and stained for endogenous IFNγ and cis-Golgi. Super-resolution structured illumination microscopy
263 (SIM) was performed using ZEN software, and PCC was quantified with Fiji. IFNγ exhibited extensive
264 colocalization with cis-Golgi in WT CTLs. No significant difference in IFNγ-Golgi PCC was observed
265 between IFNγ^{hi} and IFNγ^{lo} CTLs at 2 hours post-stimulation on day 4 (Figure 4A, B), while significantly

266 higher colocalization in IFNγ^{hi} CTLs was displayed than IFNγ^{lo} CTLs after 4 hours of re-stimulation on day
267 2 (Figure 4C, D).

268 *IFNγ localized in cytotoxic granules (CGs).* To determine whether IFNγ traffics to CGs, we analyzed IFNγ
269 and GzmB colocalization in GzmB-mTFP knock-in (KI) CTLs on days 2 and 5 post-stimulation. GzmB is a
270 marker for CGs. SIM imaging (Figure 4E, F) and Fiji-based quantification (Figure 4G, H) revealed that a
271 subset of IFNγ localized in GzmB+ CGs, with IFNγ^{hi} CTLs exhibiting significantly greater IFNγ-GzmB
272 association than IFNγ^{lo} CTLs (Figure 4F, H).

273 *Comparative localization in Golgi vs. CGs.* IFNγ showed robust cis-Golgi localization in GzmB-mTFP KI
274 CTLs, with IFNγ^{hi} CTLs displaying higher enrichment than IFNγ^{lo} CTLs (Figure 4F, H). In contrast, GzmB
275 exhibited minimal Golgi association, though IFNγ^{hi} CTLs on day 5 demonstrated slightly higher
276 GzmB-Golgi PCC than IFNγ^{lo} CTLs (Figure 4H). No such difference was observed on day 2 (Figure 4F).

277 These findings demonstrate that: The IFNγ^{hi} subset retains higher IFNγ expression and greater IFNγ
278 localization within CGs compared to IFNγ^{lo} CTLs. Newly synthesized IFNγ accumulates more prominently
279 in the Golgi apparatus than GzmB following acute TCR stimulation. The preferential trafficking of IFNγ to
280 CGs in IFNγ^{hi} CTLs suggests a direct role in cytotoxicity, consistent with their enhanced effector function.
281 IFNγ expression is dynamically regulated, with transient Golgi-associated production preceding effector
282 granule loading. Together, these data support a model wherein IFNγ^{hi} CTLs achieve superior cytotoxic
283 activity through coordinated IFNγ synthesis, Golgi processing, and granule loading.

284

285 **Temporal regulation of CRTAM and IFNγ in naive and activated CTLs**

286 To investigate the relationship between activation markers and IFNγ expression during early and late T cell
287 activation, we analyzed IFNγ, CRTAM, CD62L, CD69, and CD25 expression in wild-type CD8^{+} T cells at

288 day 0 (naive) and day 5 (activated) following TCR stimulation or restimulation.

289 *Kinetics of CRTAM and IFNγ expression.* Both CRTAM and IFNγ were upregulated upon TCR stimulation
290 (Figure 5A-F, Extended Figure 4A-C). CRTAM^{+}CTLs increased from 5.93% (1 h) to a peak of 96.6% (24 h)
291 before declining to 10.4% by 72 h, while IFNγ^{+}CTLs rose from 5.24% (1 h) to 35.6% (24 h) and
292 subsequently decreased to 9.62% (72 h) (Extended Figure 4B). MFI for both molecules peaked at 24 h and
293 became nearly undetectable by 72 h (Extended Figure 4C). Notably, day 2 and day 3 CTLs regained CRTAM
294 and IFNγ expression upon restimulation (4 h and 3 h, respectively), confirming their transient,
295 activation-dependent regulation (Extended Figure 4A).

296 *Comparative expression of CRTAM and IFNγ in naive vs. activated CTLs.* Day 5 CTLs exhibited
297 significantly higher percentage of IFNγ^{+}CTLs and IFNγ MFI than day 0 CTLs (Figure 5A-C), whereas naive
298 CTLs had a greater proportion of CRTAM^{+}CTLs (Figure 5D,E). CRTAM MFI, however, did not differ
299 significantly between day 0 and day 5 (Figure 5F). Quadrant analysis of pseudocolor plots revealed distinct
300 coexpression patterns.

301 In day 0 CTLs, only 20–25% of CRTAM^{+}CTLs expressed IFNγ, but nearly 100% of IFNγ^{+}CTLs were
302 CRTAM^{+} after 14 h stimulation (Figure 5G, I; Extended Figure 4A). In day 5 CTLs, ~71% of IFNγ^{+}CTLs
303 coexpressed CRTAM (Figure 5H, I).

304 Naive IFNγ^{+}CTLs also displayed higher CRTAM MFI than their day 5 counterparts (Figure 5J). Strikingly,
305 CRTAM^{hi} CTLs produced more IFNγ than CRTAM^{lo} subsets (Figure 5K, L), underscoring a positive
306 correlation between CRTAM and IFNγ.

307 *Activation marker dynamics.* CRTAM upregulation in naive CTLs occurred as rapidly as CD69 induction,
308 preceding CD25 expression (1–6 h; Extended Figure 4A,D,G). Conversely, CD62L levels declined
309 post-stimulation (Extended Figure 4J). By day 2, CTLs entered contraction/memory phases, marked by

310 rising CD62L and declining CD69/CD25 (Extended Figure 4E,F,I,L). With TCR restimulation, day2/3 CTLs
311 were marked with reducing CD62L and increasing CD69/CD25 (Extended Figure 4E,F,H,I,L), while the
312 percentage of CD25 didn't change (Extended Figure 4K).

313 Our findings demonstrate that CRTAM and IFNγ are transiently expressed in a TCR-dependent manner.
314 CRTAM serves as an early activation marker and correlates with IFNγ production in naive CTLs. CRTAM,
315 CD62L, CD69, and CD25 collectively define CTLs' activation states. These results position CRTAM as a
316 key early responder during primary CTLs' activation, functionally linked to IFNγ-mediated effector
317 responses.

318

319 **Discussion**

320 Effector $CD8^+$ T cells (CTLs) are central to antimicrobial and antitumor immunity, employing both lytic and
321 non-lytic cytotoxic mechanisms. While their lytic function mediated by GzmB and perforin is
322 well-characterized[30,32], the role of interferon-gamma (IFNγ) in CTL-mediated cytotoxicity remains less
323 defined. Our study elucidates the dynamic expression profile of IFNγ in activated CTLs and its functional
324 contribution to their cytotoxic potential.

325 *IFNγ dynamics and cytotoxic function.* We demonstrate that IFNγ expression in CTLs is rapidly induced
326 upon TCR activation, peaking early before declining transiently compared to the sustained expression of
327 GzmB (Figure 1A–G). This transient expression coincided with CTL maturation, as evidenced by the
328 progressive shift toward effector T cell (T_E) phenotypes and the downregulation of CD62L (Figure 2).
329 Notably, CTLs segregated into distinct $IFN\gamma^{hi}$ and $IFN\gamma^{lo}$ subsets, with the former exhibiting a stronger
330 effector phenotype (Figure 3A–C).

331 Intriguingly, $IFN\gamma^{hi}$ CTLs displayed significantly enhanced degranulation capacity (Figure 3D,G) despite

332 comparable GzmB levels to IFNγ^{lo} CTLs (Figure 3E), suggesting that IFNγ potentiates lytic cytotoxicity
333 independently of intracellular GzmB expression level. This was further supported by super-resolution
334 imaging, which revealed greater colocalization of IFNγ with GzmB-positive cytotoxic granules in IFNγ^{hi}
335 CTLs (Figure 4E–H). These findings position IFNγ not only as an immunomodulatory cytokine but also as a
336 direct contributor to the lytic efficiency of CTLs. This finding is aligned with our previous research
337 demonstrating that lytic IFNγ is stored within GzmB-containing cytotoxic granules and co-secreted at the
338 immune synapse by effector CD8^{+} T cells, a mechanism that enhances cytotoxic T lymphocytes' (CTLs)
339 killing capacity[33]. Bhat et al. (2017) demonstrated that autocrine IFNγ production by CTLs enhances their
340 motility and facilitates killing of primary target keratinocytes, both in vitro and in vivo. This finding
341 highlights the critical dependence of CD8^{+} T cell cytotoxic function on local IFNγ signaling, which has
342 important implications for immunotherapy targeting chronic viral infections and cancers[34].

343 *CRTAM as a regulator of early CTL activation.* The mechanisms governing IFNγ production in CTLs remain
344 incompletely understood. Our data highlight CRTAM as a key early activation marker that correlates with
345 IFNγ expression. CRTAM was upregulated transiently in naive CTLs upon TCR stimulation, preceding IFNγ
346 induction (Figure 5; Extended Data Figure 3). Nearly all IFNγ^{+}CTLs coexpressed CRTAM during primary
347 activation (Extended Data Figure 3A), and CRTAM^{hi} subsets produced significantly more IFNγ than
348 CRTAM^{lo} cells (Figure 5K,L).

349 The role of CRTAM in CTL biology aligns with its known functions in promoting IFNγ production in CD8^{+}
350 T cells and CD4^{+} T cells[35,36], in regulating CD4^{+} T cell polarization and in determing CD4^{+} cytotoxic T
351 lymphocyte lineage[35,37]. Its interaction with CADM1 may facilitate early CTL priming by retaining
352 activated cells in lymphoid tissues[11], while its decline in day 5 CTLs (Figure 5I,J) suggests a stage-specific
353 role in bridging early activation with effector differentiation.

354 *Future directions.* While our work establishes a link between IFNγ expression and CTL cytotoxicity, the
355 molecular pathways connecting CRTAM to IFNγ regulation warrant further investigation. Single-cell RNA
356 sequencing could delineate the transcriptional programs distinguishing IFNγ^{hi} and IFNγ^{lo} subsets[38–40],
357 offering insights into their functional specialization. Additionally, mechanistic studies are needed to clarify
358 whether IFNγ enhances lytic function through granule trafficking and fusion, target cell sensitization, or
359 other effector pathways.

360

361 # Conclusions

362 In conclusion, the expression of IFNγ and GzmB shows a maturation-dependent pattern but dfifferent
363 kinetics. Unlike GzmB, IFNγ production is rapid and transient following TCR (re)activation and does not
364 require mature immune synapse formation. We further demonstrate that CD62L downregulation and CD69
365 upregulation serve as robust markers of TCR-driven transition from central memory (T_{CM}) to effector
366 memory (T_{EM}) phenotypes. Functionally, IFNγ may enhance CTL cytotoxicity by promoting
367 Golgi-dependent processing and efficient sorting into lytic granules, with elevated IFNγ levels correlating
368 with greater killing capacity. Additionally, we identify CRTAM as a critical early responder in primary CTL
369 activation, where it may regulate initial IFNγ expression and contribute to IFNγ-mediated effector functions.
370 Collectively, these insights establish a mechanistic framework for refining T cell-based immunotherapies
371 against infectious diseases and malignancies.

372

373 **Abbreviations**

374 CTL: CD8+ T lymphocyte; IFNγ:interferon-gamma; IFNγ^{hi}: IFNγ^{high} subset; IFNγ^{lo}: IFNγ^{low} subset; WT:
375 Wild-type; GzmB-mTFP KI: Granzyme B-mTFP Knock-in; TCR: T-cell receptor; T_N: Naive CD8+ T cells;

376 T_E/T_{EM}: Effector/effector memory T cells; T_{CM}: Central memory T cells; T_{EX}: T cell exhaustion; CGs:
377 Cytotoxic granules; SGs: Secretory lysosomes; CD44: Homing Cell Adhesion Molecule; CD62L: L-selectin;
378 CD25: Interleukin-2 receptor; CD127: IL-7 receptor alpha; LAMPs: Lysosome-associated membrane
379 glycoproteins; CD107a (LAMP-1), CD107b (LAMP-2), and CD63 (LAMP-3); FasL/CD95L: Fas ligand; Fas:
380 Fas receptor; CRTAM: Class I-restricted T cell-associated molecule; DPBS: Dulbecco's Phosphate-Buffered
381 Saline; BME: β-Mercaptoethanol; IF: immunofluorescence; ICC: immunocytochemistry; FC: Flow
382 cytometry; TNFα: Tumor necrosis factor-alpha; IL-6: Interleukin-6; SIM: Structured illumination
383 microscopy; IRF-1: Interferon regulatory factor-1; MFI: Median fluorescence intensity; PCC: Pearson's
384 correlation coefficient.

385

386 **Acknowledgments**

387 We thank Anja Bergsträßer, Margarete Klose, Nicole Rothgerber and Katrin Sandmeier for excellent
388 technical assistance.

389

390 **Author Contributions**

391 VP and XL conceived and designed the study. XL conducted flow cytometry experiments and performed
392 data analysis. XL carried out structured illumination microscopy (SIM) imaging and completed
393 co-localization analysis. JR, VP, and XL secured funding for the research. EK and H-FC provided critical
394 insights for data interpretation. EK and VP offered technical support for flow cytometry and structured
395 illumination microscopy. XL drafted the manuscript with input from all authors. All authors reviewed, edited,
396 and approved the final version of the manuscript.

397

Funding

This work was supported by China Scholarship Council (201808080081), grants from the Deutsche Forschungsgemeinschaft (SFB 894 (2011-2022) A10 to J. R. and V. P., H.-F. Chang & E. Krause since 2022), and the Postdoctoral Project Funding from the First Affiliated Hospital of Chongqing Medical University (0303020203T0597).

Availability of data and materials

Additional data and information that support the findings of this study are available from the corresponding author upon reasonable request.

Ethics approval and consent to participate

All experimental procedures were conducted in compliance with regulations of the state of Saarland (Landesamt für Verbraucherschutz, AZ.: 2.4.1.1 and 11/2021).

Consent for publication

Not applicable.

Competing interests

The authors declare no competing interests.

418 **Author details**

419 [1] Department of Neurology, NHC Key Laboratory of Diagnosis and Treatment on Brain Functional Diseases,

420 The First Affiliated Hospital of Chongqing Medical University, No.1 Youyi Road, Yuzhong District,

421 Chongqing, 400016, China

422 [2] Cellular Neurophysiology, Center for Integrative Physiology and Molecular Medicine, (CIPMM), Saarland

423 University, 66421 Homburg, Germany

424

425 # References

426 [1] Weninger W, Manjunath N, von Andrian UH. Migration and differentiation of CD8+ T cells. *Immunol*
427 *Rev*. 2002 Aug;186:221-33. doi: 10.1034/j.1600-065x.2002.18618.x. PMID: 12234374

428 [2] [2] Stemberger C, Huster KM, Koffler M, Anderl F, Schiemann M, Wagner H, Busch DH. A single naive
429 CD8+ T cell precursor can develop into diverse effector and memory subsets. *Immunity*. 2007
430 Dec;27(6):985-97. doi: 10.1016/j.immuni.2007.10.012. PMID: 18082432

431 [3] Jameson SC, Masopust D. Diversity in T cell memory: an embarrassment of riches. *Immunity*. 2009 Dec
432 18;31(6):859-71. doi: 10.1016/j.immuni.2009.11.007. PMID: 20064446

433 [4] Sallusto F, Lenig D, Förster R, Lipp M, Lanzavecchia A. Two subsets of memory T lymphocytes with
434 distinct homing potentials and effector functions. *Nature*. 1999 Oct 14;401(6754):708-12. doi:
435 10.1038/44385. PMID: 10537110

436 [5] Sallusto F, Geginat J, Lanzavecchia A. Central memory and effector memory T cell subsets: function,
437 generation, and maintenance. *Annu Rev Immunol.* 2004;22:745-63. doi:
438 10.1146/annurev.immunol.22.012703.104702. PMID: 15032595

439 [6] Huster KM, Busch V, Schiemann M, Linkemann K, Kerksiek KM, Wagner H, Busch DH. Selective
440 expression of IL-7 receptor on memory T cells identifies early CD40L-dependent generation of distinct
441 CD8+ memory T cell subsets. *Proc Natl Acad Sci U S A.* 2004 Apr 13;101(15):5610-5. doi:
442 10.1073/pnas.0308054101. Epub 2004 Mar 25. PMID: 15044705

443 [7] Wherry EJ. T cell exhaustion. *Nat Immunol.* 2011 Jun;12(6):492-9. doi: 10.1038/ni.2035. PMID:
444 21739672.

445 [8] Koh CH, Lee S, Kwak M, Kim BS, Chung Y. CD8 T-cell subsets: heterogeneity, functions, and
446 therapeutic potential. *Exp Mol Med.* 2023 Nov;55(11):2287-2299. doi: 10.1038/s12276-023-01105-x.

447 Epub 2023 Nov 1. PMID: 37907738; PMCID: PMC10689838.

448 [9] Weigelin B, den Boer AT, Wagena E, Broen K, Dolstra H, de Boer RJ, Figdor CG, Textor J, Friedl P.
449 Cytotoxic T cells are able to efficiently eliminate cancer cells by additive cytotoxicity. *Nat Commun.*
450 2021 Sep 1;12(1):5217. doi: 10.1038/s41467-021-25282-3. PMID: 34471116; PMCID: PMC8410835.

451 [10] Perdomo-Celis F, Taborda NA, Rugeles MT. CD8+ T-Cell Response to HIV Infection in the Era of
452 Antiretroviral Therapy. *Front Immunol.* 2019 Aug 9;10:1896. doi: 10.3389/fimmu.2019.01896. PMID:
453 31447862

454 [11] Takeuchi A, Itoh Y, Takumi A, Ishihara C, Arase N, Yokosuka T, Koseki H, Yamasaki S, Takai Y,
455 Miyoshi J, Ogasawara K, Saito T. CRTAM confers late-stage activation of CD8+ T cells to regulate
456 retention within lymph node. *J Immunol.* 2009 Oct 1;183(7):4220-8. doi: 10.4049/jimmunol.0901248.
457 Epub 2009 Sep 14. PMID: 19752223

458 [12] Cruz-Guilloty F, Pipkin ME, Djuretic IM, Levanon D, Lotem J, Lichtenheld MG, Groner Y, Rao A.
459 Runx3 and T-box proteins cooperate to establish the transcriptional program of effector CTLs. *J Exp*
460 *Med.* 2009 Jan 16;206(1):51-9. doi: 10.1084/jem.20081242. Epub 2009 Jan 12. PMID: 19139168

461 [13] Paley MA, Kroy DC, Odorizzi PM, Johnnidis JB, Dolfi DV, Barnett BE, Bikoff EK, Robertson EJ,
462 Lauer GM, Reiner SL, Wherry EJ. Progenitor and terminal subsets of CD8+ T cells cooperate to contain
463 chronic viral infection. *Science*. 2012 Nov 30;338(6111):1220-5. doi: 10.1126/science.1229620. PMID:
464 23197535

465 [14] Betts MR, Koup RA. Detection of T-cell degranulation: CD107a and b. *Methods Cell Biol.*
466 2004;75:497-512. doi: 10.1016/s0091-679x(04)75020-7. PMID: 15603439

467 [15] Peters PJ, Borst J, Oorschot V, Fukuda M, Krähenbühl O, Tschopp J, Slot JW, Geuze HJ. Cytotoxic T
468 lymphocyte granules are secretory lysosomes, containing both perforin and granzymes. *J Exp Med.*
469 1991 May 1;173(5):1099-109. doi: 10.1084/jem.173.5.1099. PMID: 2022921

470 [16] Fukuda M. Lysosomal membrane glycoproteins. Structure, biosynthesis, and intracellular trafficking. *J*
471 *Biol Chem.* 1991 Nov 15;266(32):21327-30. PMID: 1939168

472 [17] Bossi G, Griffiths GM. Degranulation plays an essential part in regulating cell surface expression of Fas
473 ligand in T cells and natural killer cells. *Nat Med.* 1999 Jan;5(1):90-6. doi: 10.1038/4779. PMID:
474 9883845

475 [18] Kambayashi T, Assarsson E, Lukacher AE, Ljunggren HG, Jensen PE. Memory CD8+ T cells provide
476 an early source of IFN-gamma. *J Immunol.* 2003 Mar 1;170(5):2399-408. doi:
477 10.4049/jimmunol.170.5.2399. PMID: 12594263

478 [19] Ivashkiv LB. IFNγ: signalling, epigenetics and roles in immunity, metabolism, disease and cancer
479 immunotherapy. *Nat Rev Immunol.* 2018 Sep;18(9):545-558. doi: 10.1038/s41577-018-0029-z. PMID:
480 29921905

481 [20] Bold TD, Ernst JD. CD4+ T cell-dependent IFN-γ production by CD8+ effector T cells in
482 Mycobacterium tuberculosis infection. *J Immunol.* 2012 Sep 1;189(5):2530-6. doi:
483 10.4049/jimmunol.1200994. Epub 2012 Jul 25. PMID: 22837486

484 [21] Costa-Pereira AP, Williams TM, Strobl B, Watling D, Briscoe J, Kerr IM. The antiviral response to
485 gamma interferon. *J Virol.* 2002 Sep;76(18):9060-8. doi: 10.1128/jvi.76.18.9060-9068.2002. PMID:
486 12186889

487 [22] Rhein BA, Powers LS, Rogers K, Anantpadma M, Singh BK, Sakurai Y, Bair T, Miller-Hunt C, Sinn P,
488 Davey RA, Monick MM, Maury W. Interferon-γ Inhibits Ebola Virus Infection. *PLoS Pathog.* 2015
489 Nov 12;11(11):e1005263. doi: 10.1371/journal.ppat.1005263. PMID: 26562011

490 [23] Gocher AM, Workman CJ, Vignali DAA. Interferon-γ: teammate or opponent in the tumour
491 microenvironment? *Nat Rev Immunol.* 2022 Mar;22(3):158-172. doi: 10.1038/s41577-021-00566-3.
492 Epub 2021 Jun 21. PMID: 34155388; PMCID: PMC8688586

493 [24] Mazet JM, Mahale JN, Tong O, Watson RA, Lechuga-Vieco AV, Pirgova G, Lau VWC, Attar M,
494 Koneva LA, Sansom SN, Fairfax BP, Gérard A. IFNγ signaling in cytotoxic T cells restricts anti-tumor
495 responses by inhibiting the maintenance and diversity of intra-tumoral stem-like T cells. *Nat Commun.*
496 2023 Jan 19;14(1):321. doi: 10.1038/s41467-023-35948-9. PMID: 36658158; PMCID: PMC9852295

497 [25] Jorgovanovic D, Song M, Wang L, Zhang Y. Roles of IFN-γ in tumor progression and regression: a
498 review. *Biomark Res.* 2020 Sep 29;8:49. doi: 10.1186/s40364-020-00228-x. PMID: 33005420

499 [26] Yang MQ, Du Q, Varley PR, Goswami J, Liang Z, Wang R, Li H, Stolz DB, Geller DA. Interferon
500 regulatory factor 1 priming of tumour-derived exosomes enhances the antitumour immune response. *Br*
501 *J Cancer.* 2018 Jan;118(1):62-71. doi: 10.1038/bjc.2017.389. Epub 2017 Nov 7. PMID: 29112686

502 [27] Karki R, Sharma BR, Tuladhar S, Williams EP, Zalduondo L, Samir P, Zheng M, Sundaram B, Banoth B,
503 Malireddi RKS, Schreiner P, Neale G, Vogel P, Webby R, Jonsson CB, Kanneganti TD. Synergism of
504 TNF-α and IFN-γ Triggers Inflammatory Cell Death, Tissue Damage, and Mortality in SARS-CoV-2
505 Infection and Cytokine Shock Syndromes. *Cell.* 2021 Jan 7;184(1):149-168.e17. doi:
506 10.1016/j.cell.2020.11.025. Epub 2020 Nov 19. PMID: 33278357

507 [28] Lochhead RB, Strle K, Arvikar SL, Weis JJ, Steere AC. Lyme arthritis: linking infection, inflammation
508 and autoimmunity. *Nat Rev Rheumatol.* 2021 Aug;17(8):449-461. doi: 10.1038/s41584-021-00648-5.
509 Epub 2021 Jul 5. PMID: 34226730

510 [29] Glass CK, Natoli G. Molecular control of activation and priming in macrophages. *Nat Immunol.* 2016
511 Jan;17(1):26-33. doi: 10.1038/ni.3306. PMID: 26681459

512 [30] Chitirala P, Chang HF, Martzloff P, Harenberg C, Ravichandran K, Abdulreda MH, Berggren PO,
513 Krause E, Schirra C, Leinders-Zufall T, Benseler F, Brose N, Rettig J. Studying the biology of cytotoxic
514 T lymphocytes in vivo with a fluorescent granzyme B-mTFP knock-in mouse. *Elife.* 2020 Jul
515 22;9:e58065. doi: 10.7554/eLife.58065. PMID: 32696761

516 [31] Estl M, Blatt P, Li X, Becherer U, Chang HF, Rettig J, Pattu V. Various Stages of Immune Synapse
517 Formation Are Differently Dependent on the Strength of the TCR Stimulus. *Int J Mol Sci*. 2020 Apr
518 2;21(7):2475. doi: 10.3390/ijms21072475. PMID: 32252488

519 [32] Dustin ML, Long EO. Cytotoxic immunological synapses. *Immunol Rev.* 2010 May;235(1):24-34. doi:
520 10.1111/j.0105-2896.2010.00904.x. PMID: 20536553

521 [33] Li X, Schirra C, Wirkner ML, Tu SM, Lin CH, Hohmann M, Alawar N, Chouaib A, Becherer U, Pattu V,
522 Rettig J, Krause E, Chang HF. Lytic IFNγ is stored in granzyme B-containing cytotoxic granules and
523 co-secreted by effector $CD8^+$ T cells. *BioRxiv* 2025.01.29.635520; doi:
524 https://doi.org/10.1101/2025.01.29.635520

525 [34] Bhat P, Leggatt G, Waterhouse N, Frazer IH. Interferon-γ derived from cytotoxic lymphocytes directly
526 enhances their motility and cytotoxicity. *Cell Death Dis.* 2017 Jun 1;8(6):e2836. doi:
527 10.1038/cddis.2017.67. PMID: 28569770; PMCID: PMC5520949.

528 [35] Yeh JH, Sidhu SS, Chan AC. Regulation of a late phase of T cell polarity and effector functions by
529 Crtam. *Cell*. 2008 Mar 7;132(5):846-59. doi: 10.1016/j.cell.2008.01.013. PMID: 18329370

530 [36] Boles KS, Barchet W, Diacovo T, Cella M, Colonna M. The tumor suppressor TSLC1/NECL-2 triggers
531 NK-cell and CD8+ T-cell responses through the cell-surface receptor CRTAM. *Blood*. 2005 Aug
532 1;106(3):779-86. doi: 10.1182/blood-2005-02-0817. Epub 2005 Apr 5. PMID: 15811952

533 [37] Takeuchi A, Badr Mel S, Miyauchi K, Ishihara C, Onishi R, Guo Z, Sasaki Y, Ike H, Takumi A, Tsuji
534 NM, Murakami Y, Katakai T, Kubo M, Saito T. CRTAM determines the CD4+ cytotoxic T lymphocyte
535 lineage. *J Exp Med*. 2016 Jan 11;213(1):123-38. doi: 10.1084/jem.20150519. Epub 2015 Dec 22. PMID:
536 26694968;

537 [38] Speiser DE, Wieckowski S, Gupta B, Iancu EM, Baumgaertner P, Baitsch L, Michielin O, Romero P,
538 Rufer N. Single cell analysis reveals similar functional competence of dominant and nondominant CD8
539 T-cell clonotypes. *Proc Natl Acad Sci U S A*. 2011 Sep 13;108(37):15318-23. doi:
540 10.1073/pnas.1105419108. Epub 2011 Aug 29. PMID: 21876175

541 [39] Giles JR, Ngiow SF, Manne S, Baxter AE, Khan O, Wang P, Staupe R, Abdel-Hakeem MS, Huang H,
542 Mathew D, Painter MM, Wu JE, Huang YJ, Goel RR, Yan PK, Karakousis GC, Xu X, Mitchell TC,
543 Huang AC, Wherry EJ. Shared and distinct biological circuits in effector, memory and exhausted CD8+
544 T cells revealed by temporal single-cell transcriptomics and epigenetics. *Nat Immunol*. 2022
545 Nov;23(11):1600-1613. doi: 10.1038/s41590-022-01338-4. Epub 2022 Oct 21. PMID: 36271148

546 [40] Xue Z, Wu L, Tian R, Gao B, Zhao Y, He B, Sun D, Zhao B, Li Y, Zhu K, Wang L, Yao J, Liu W, Lu L.
547 Integrative mapping of human CD8+ T cells in inflammation and cancer. *Nat Methods*. 2025
548 Feb;22(2):435-445. doi: 10.1038/s41592-024-02530-0. Epub 2024 Nov 29. PMID: 39614111.

549 [41] Bzeih H (2016) The Role of Synaptobrevin2 in Exo-Endocytosis in Primary Mouse Cytotoxic
550 lymphocytes.

551 **Figure Legends**

552 **Figure 1 | Intracellular IFNγ and granzyme B (GzmB) expression in activated CTLs. (A–D)** WT CTLs
553 (days 3–5 post-activation) were re-stimulated with plate-bound anti-CD3e antibody (10 μg/mL) and analyzed
554 for intracellular IFNγ and GzmB expression over 0–4 h. **(A, B)** Pseudocolor plots depict fluorescence
555 intensity of rat anti-mouse IFNγ-Alexa488 (x-axis) and GzmB-Alexa647 (x-axis) against side scatter area
556 (SSC-A, y-axis). **(C, D)** Median fluorescence intensity (MFI) of IFNγ-Alexa488 and GzmB-Alexa647. **(E, F)**
557 Temporal changes in IFNγ and GzmB expression in re-stimulated CTLs. MFI dynamics of IFNγ-Alexa488
558 and GzmB-Alexa647. Data are mean ± SEM (N ≥ 3). Statistical significance was determined by one-way
559 ANOVA and unpaired t-test (*$p < 0.05$, **$p < 0.01$, ***$p < 0.001$; NS, not significant).

560

561 **Figure 2 | Surface activation marker expression profiles in CTLs analyzed by flow cytometry. (A–C)**
562 WT CTLs (days 3–5 post-activation) were re-stimulated with plate-bound anti-CD3e antibody (10 μg/mL)
563 for 0–4 h and stained for CD44 and CD62L. **(A)** Pseudocolor plots depict fluorescence intensity of rat
564 anti-mouse CD62L-APC (x-axis) and CD44-PE (y-axis). **(B, C)** Frequencies of T_E and T_{CM} populations. **(D,**
565 **E)** WT CTLs (day 5 post-activation) were re-stimulated with plate-bound anti-CD3e (10 μg/mL) for 2 h
566 and analyzed for multiple activation markers. **(D)** Fold change in CD44+, CD62L+, CD25+, and CD69+ cell
567 populations. **(E)** MFI change of CD44-PE, CD62L-APC, CD25-PE, and CD69-APC before and after 2 h
568 restimulation. Data represent mean ± SEM (N ≥ 3). Statistical analysis was performed using one-way
569 ANOVA and unpaired t-test (*$p < 0.05$, **$p < 0.01$, ***$p < 0.001$; NS, not significant).

570

571 **Figure 3 | Characterization of IFNγ^{hi} and IFNγ^{lo} CTL subsets and their cytotoxic potential. (A-E)** WT
572 CTLs were re-stimulated with plate-bound anti-CD3e antibody for 0-4 h and processed for flow cytometry
573 analysis: One aliquot was surface-stained with anti-CD44-APC and anti-CD62L-PE, followed by

574 intracellular staining for IFNγ-Alexa488. Another aliquot was intracellularly stained for IFNγ-Alexa488 and
575 GzmB-Alexa647 **(A)** Gating strategy and surface marker expression profiles of IFNγ^{hi} vs IFNγ^{lo} CTLs. **(B)**
576 Percentage of effector T cells (T_E) in each subset. **(C)** Percentage of central memory T cells (T_{CM}) in each
577 subset. **(D)** IFNγ fluorescence intensity in IFNγ^{hi} vs IFNγ^{lo} subsets. **(E)** GzmB fluorescence intensity in
578 IFNγ^{hi} vs IFNγ^{lo} subsets. **(F,G)** Degranulation capacity assessed by CD107a surface expression: Day 3 and 5
579 WT CTLs were stimulated with plate-bound anti-CD3e for 3 h in the presence of anti-CD107a-PE, followed
580 by intracellular IFNγ staining. **(F)** Percentage of CD107a+ CTLs pre- and post-stimulation. **(G) i,iii**: CD107a
581 expression in IFNγ^{hi} vs IFNγ^{lo} CTLs at day 3 and 5. **ii,iv**: CD107a fluorescence intensity in IFNγ^{hi} vs IFNγ^{lo}
582 CTLs at day 3 and 5. Data represent mean ± SEM (N≥2 independent experiments). Statistical significance
583 was determined by unpaired t-test (**p*<0.05, ***p*<0.01, ****p*<0.001).
584
585 **Figure 4 | Subcellular localization of IFNγ in IFNγ^{hi} and IFNγ^{lo} CTL subsets. (A-H)** WT or GzmB-mTFP
586 KI CTLs were re-stimulated with plate-bound anti-CD3e (10 µg/mL) (for day2: 4 h restimulation, day4 and
587 day 5: 2 h restimulation) and processed for super-resolution microscopy (SIM): Imaging and analysis: Cells
588 were stained for IFNγ, GzmB, and cis-Golgi marker (GM130) IFNγ^{hi} vs IFNγ^{lo} subsets were imaged using
589 optimized laser power and EMCCD gain settings. Colocalization analysis performed using Fiji-win64
590 software. Quantitative comparisons and graphing performed using GraphPad Prism 10.2.3. Experimental
591 details: **(A-B)** Day 4 WT CTLs: Primary antibodies: Rat anti-mouse IFNγ-Alexa488 (1:200), mouse
592 anti-GM130 (1:100). Secondary antibody: Goat anti-mouse-Alexa647 (1:1000). **(B)** Pearson's correlation
593 coefficient for IFNγ and cis-Golgi colocalization. **(C-D)** Day 2 WT CTLs: Primary antibodies: Rat
594 anti-mouse IFNγ (1:200), mouse anti-GM130 (1:100). Secondary antibodies: Alexa647 chicken anti-rat IgG
595 (1:800), Alexa568 goat anti-mouse IgG (1:400). Imaging parameters: IFNγ^{lo}: 561 nm laser (1.5%, gain 80);
596 647 nm laser (1.5%, gain 50). IFNγ^{hi}: 561 nm laser (1.2%, gain 80); 647 nm laser (0.6%, gain 25). **(D)**

597 Pearson's correlation coefficient analysis. **(E-H)** GzmB-mTFP KI CTLs: Primary antibodies: Rat anti-mouse
598 IFNγ (1:200), mouse anti-GM130 (1:100). Secondary antibodies: Alexa647 chicken anti-rat IgG (1:800),
599 Alexa568 goat anti-mouse IgG (1:400). **(E,F)** Day 2 CTLs imaging parameters: IFNγ^{hi}: 488 nm (22%, gain
600 80); 568 nm (1.2%, gain 80); 647 nm (0.7%, gain 40). IFNγ^{lo}: 488 nm (26%, gain 80); 568 nm (1.2%, gain
601 80); 647 nm (1.5%, gain 80). **(G,H)** Day 5 CTLs imaging parameters: IFNγ^{hi}: 488 nm (18%, gain 80); 561
602 nm (1.2%, gain 80); 647 nm (0.3%, gain 20). IFNγ^{lo}: 488 nm (16%, gain 80); 561 nm (1.5%, gain 80); 647
603 nm (1.0%, gain 80). **(F,H)** Pearson's correlation coefficient analyses. Statistical analysis: Data represent
604 mean ± SEM. Significance was determined by one-way ANOVA with t-tests (*p<0.05, **p<0.01,
605 ***p<0.001; NS, not significant).
606
607 **Figure 5 | Co-expression analysis of CRTAM and IFNγ in activated CTLs by flow cytometry.**
608 Experimental design: Day 0 CTLs: Stimulated with plate-bound anti-CD3e (10 μg/mL) and anti-CD28 (5
609 μg/mL) for 14 h. Day 5 CTLs: Re-stimulated with plate-bound anti-CD3e (10 μg/mL) for 2 h in 96-well
610 plates. Staining: Anti-CRTAM-PE and anti-IFNγ-Alexa488 antibodies. Flow cytometry analysis: **(A)**
611 Representative pseudocolor plots of IFNγ expression in day 0 vs day 5 CTLs. **(B)** Frequency of IFNγ^{+}CTLs.
612 **(C)** MFI of IFNγ-Alexa488. **(D)** Representative pseudocolor plots of CRTAM expression. **(E)** Frequency of
613 CRTAM^{+}CTL populations. **(F)** MFI of CRTAM-PE. Co-expression analysis: **(G, H)** Quadrant plots showing
614 IFNγ and CRTAM co-expression patterns. **(I)** Frequency of CRTAM^{+} cells in IFNγ^{+} CTLs. **(J)** MFI of
615 CRTAM-PE in IFNγ^{+}CTLs. **(K-L)** MFI of IFNγ-Alexa488 in CRTAM^{hi} vs CRTAM^{lo} subsets. Statistical
616 analysis: Data represent mean ± SEM (N=3 independent experiments). Significance was determined by
617 unpaired t-test (*p<0.05, **p<0.01, ***p<0.001; NS, not significant).
618
619

620 **Additional information**

621 **Extended Data Table 1 | Antibodies used in this study**

Antibody, anti-	Supplier	Clone	Host	Dilution	Application
Mouse CD3e	BD Pharmingen	145-2C11	Hamster	1:100	Plate/glass coating
Mouse IFNγ	Biolegend	XMG1.2	Rat	1:200	FC, ICC
Mouse IFNγ-Alexa488	Biolegend	XMG1.2	Rat	1:200	FC, ICC
Mouse GzmB-Alexa647	Biolegend	GB11	Rat	1:200	FC, ICC
Mouse-CRTAM-PE	Biolegend	11-5	Rat	1:200	FC
Mouse-CD25-FITC	BD Pharmingen	7D4	Rat	1:200	FC
Mouse-CD44-PE	BD Bioscience	IM7	Rat	1:1200	FC
Mouse-CD62L-APC	BD Bioscience	MEL-14 (RUO)	Rat	1:1600	FC
Cis Golgi	BD Bioscience	GM 130	Mouse	1:100	ICC
Mouse-CD107a-PE	BD Bioscience	(1D4B)	Rat	1:200	FC
Mouse-CD69-APC	Thermo Scientific	H1.2F3	Hamst	1:100	FC
Mouse-IgG-Alexa647	Thermo Scientific	—	Goat	1:1000	ICC
Rat-IgG-Alexa647	Thermo Scientific	—	Chicken	1:800	ICC
Mouse-IgG-Alexa568	Thermo Scientific	—	Goat	1:400	ICC

622 **Note:** FC: flow cytometry, ICC: immunocytochemistry.

623

624 **Extended Data**

625 **Extended Data Figure 1 | Dynamic expression profiles of CD44 and CD62L in reactivated CTLs.** WT

626 cytotoxic T lymphocytes (CTLs) activated for 3-5 days were re-stimulated with plate-bound anti-CD3e

627 antibody (10 μg/mL) for the indicated durations (0, 0.5, 1, 2, 3, and 4 hours), followed by intracellular
628 staining for IFNγ and granzyme B (GzmB). **(A, C)** Fold change in the percentage of CD44+ and CD62L+
629 cells. (**B,D)** Median fluorescence intensity (MFI) of CD44-PE (rat anti-mouse) and CD62L-APC (rat
630 anti-mouse). Data represent mean ± SEM from ≥3 independent experiments. Statistical significance was
631 determined by one-way ANOVA with post hoc unpaired t-tests: NS, $p > 0.05$; *$0.01 < p \leq 0.05$; **$0.001 < p$
632 ≤ 0.01; ***$0.0001 < p \leq 0.001$.
633
634 **Extended Data Figure 2 | Flow cytometric analysis of T cell activation markers.** WT cytotoxic T
635 lymphocytes (CTLs) activated for 3–5 days were re-stimulated with plate-bound anti-CD3e antibody (10
636 μg/mL) for 0–4 hours and stained for surface expression of CD44 and CD62L. (**A)** Median fluorescence
637 intensity (MFI) of CD44-PE (rat anti-mouse) in CD44+ IFNγ^{hi} and IFNγ^{lo} CTLs. (**B)** MFI of CD62L-APC
638 (rat anti-mouse) in CD62L+ IFNγ^{hi} and IFNγ^{lo} CTLs. Data represent mean ± SEM from ≥3 independent
639 experiments. Statistical analysis was performed using one-way ANOVA followed by unpaired t-tests: NS,
640 $p > 0.05$; *$0.01 < p \leq 0.05$; **$0.001 < p \leq 0.01$; ***$0.0001 < p \leq 0.001$.
641
642 **Extended Data Figure 3 | Temporal dynamics of IFNγ and granzyme B expression in activated CTLs.**
643 WT cytotoxic T lymphocytes (CTLs) activated for 4 days were re-stimulated with plate-bound anti-CD3e
644 monoclonal antibody (10 μg/mL) for 4–24 hours. Cells were subsequently stained for intracellular IFNγ and
645 GzmB using fluorescently labeled antibodies and analyzed by flow cytometry (FlowJo v10.10.0). (**A)** IFNγ
646 fluorescence intensity changes in IFNγ^{hi} and IFNγ^{lo} subsets. (**B)** GzmB fluorescence intensity changes in
647 IFNγ^{hi} and IFNγ^{lo} subsets. Data represent mean ± SEM from 3 independent experiments. Statistical
648 significance was determined by one-way ANOVA followed by unpaired t-tests: NS, $p > 0.05$, *$0.01 < p \leq$
649 0.05, **$0.001 < p \leq 0.01$, ***$0.0001 < p \leq 0.001$.

650

651 **Extended Data Figure 4 | Temporal profiling of activation markers and IFNγ expression in primary**

652 **CTLs.** Day 0 WT cytotoxic T lymphocytes (CTLs) were stimulated in 96-well plates with plate-bound

653 anti-CD3e (10 μg/mL) and anti-CD28 (5 μg/mL) antibodies for 0 h, 3 h, 6 h, 14 h, 24 h, 48 h,and 72 h ,

654 followed by surface staining for CRTAM, CD62L, CD69, and CD25, and intracellular staining for IFNγ. **(A)**

655 Pseudocolor plots showing temporal expression patterns of CRTAM and IFNγ in day 0 CTLs following

656 stimulation. (**D, G, J)** Pseudocolor plots depicting dynamic expression of CD62L, CD69, and CD25 in day 0

657 CTLs. **(B, E, H, K)** Quantification of CRTAM+, IFNγ+, CD62L+, CD69+, and CD25+ cell populations in

658 stimulated day 0 CTLs. **(C, F, I, L)** Quantification of CRTAM-PE, IFNγ-Alexa488, CD62L-APC,

659 CD69-APC, and CD25-PE median fluorescence intensity. Data represent mean ± SEM.

660

661

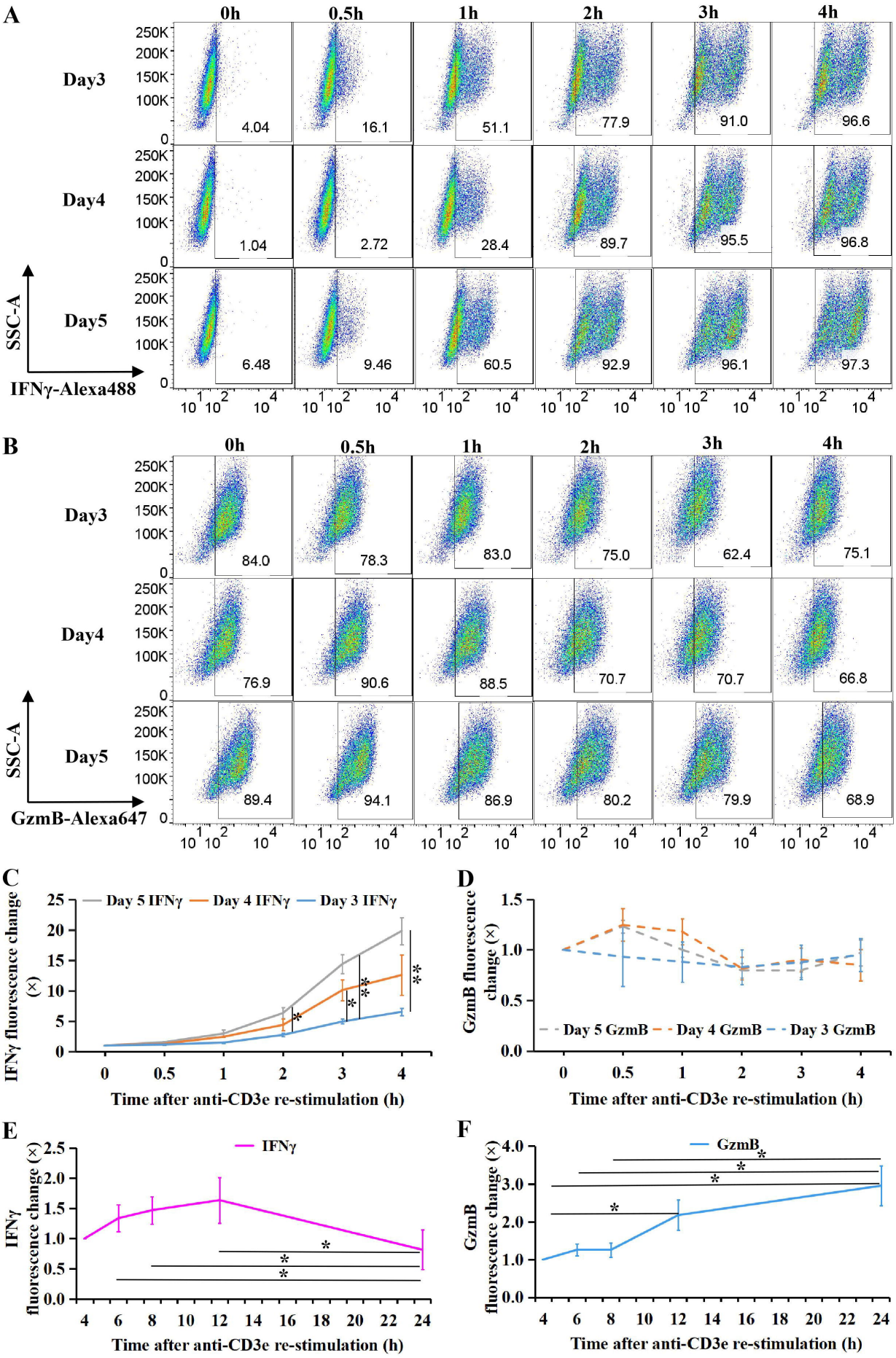
A
0h
0.5h
1h
2h
3h
4h
Day3
Day4
Day5
SSC-A
IFNγ-Alexa488
4.04
16.1
51.1
77.9
91.0
96.6
1.04
2.72
28.4
89.7
95.5
96.8
6.48
9.46
60.5
92.9
96.1
97.3
B
GzmB-Alexa647
84.0
78.3
83.0
75.0
62.4
75.1
76.9
90.6
88.5
70.7
70.7
66.8
89.4
94.1
86.9
80.2
79.9
68.9
C
IFNγ fluorescence change (×)
Day 5 IFNγ
Day 4 IFNγ
Day 3 IFNγ
Time after anti-CD3e re-stimulation (h)
D
GzmB fluorescence change (×)
Day 5 GzmB
Day 4 GzmB
Day 3 GzmB
Time after anti-CD3e re-stimulation (h)
E
IFNγ fluorescence change (×)
IFNγ
Time after anti-CD3e re-stimulation (h)
F
GzmB fluorescence change (×)
GzmB
Time after anti-CD3e re-stimulation (h)

Figure 1

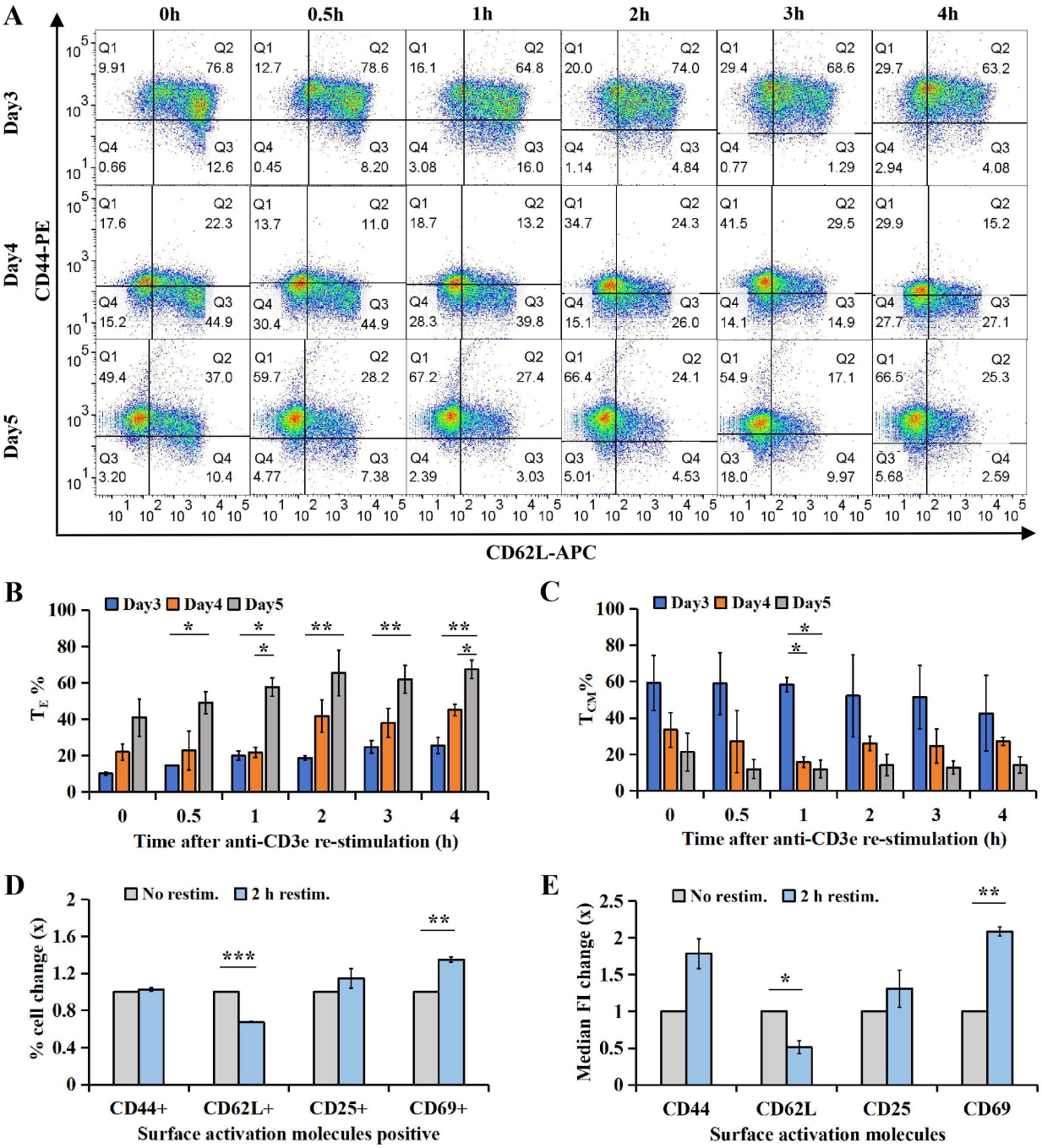
A
0h
0.5h
1h
2h
3h
4h
Day3
Day4
Day5
CD44-PE
CD62L-APC
B
Day3 Day4 Day5
T_E %
Time after anti-CD3e re-stimulation (h)
C
Day3 Day4 Day5
T_{CM} %
Time after anti-CD3e re-stimulation (h)
D
No restim. 2 h restim.
% cell change (x)
CD44+ CD62L+ CD25+ CD69+
Surface activation molecules positive
E
No restim. 2 h restim.
Median FI change (x)
CD44 CD62L CD25 CD69
Surface activation molecules

Figure 2

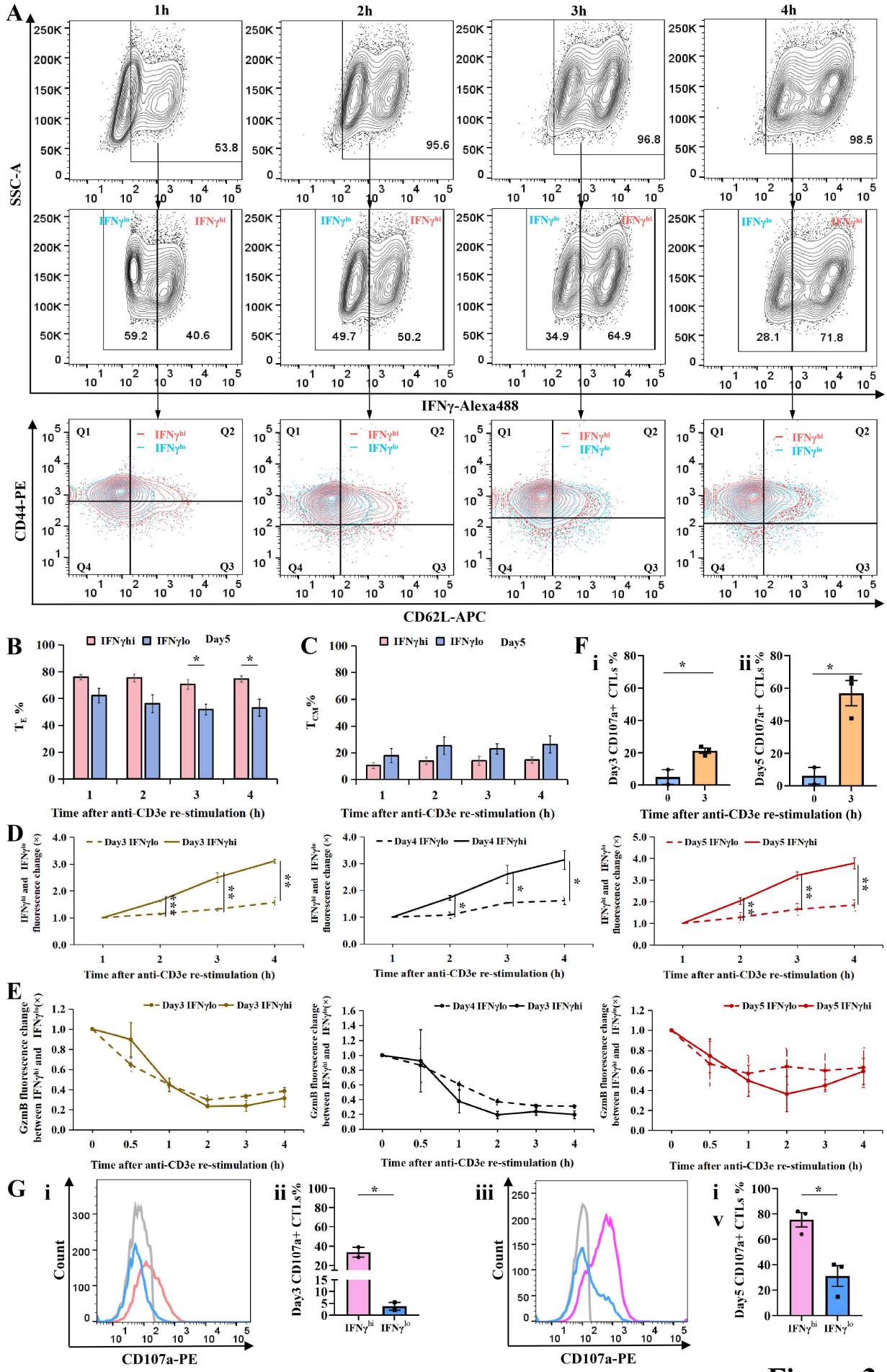
A
1h
2h
3h
4h
SSC-A
53.8
95.6
96.8
98.5
IFNγlo
IFNγhi
59.2
40.6
49.7
50.2
34.9
64.9
28.1
71.8
IFNγ-Alexa488
Q1
Q2
Q3
Q4
CD44-PE
CD62L-APC
B
IFNγhi
IFNγlo
Day5
T_E %
Time after anti-CD3e re-stimulation (h)
C
T_CM %
F
i
ii
Day3 CD107a+ CTLs %
Day5 CD107a+ CTLs %
D
Day3 IFNγlo
Day3 IFNγhi
Day4 IFNγlo
Day4 IFNγhi
Day5 IFNγlo
Day5 IFNγhi
IFNγhi and IFNγlo fluorescence change (×)
E
GzmB fluorescence change between IFNγhi and IFNγlo(×)
G
i
ii
iii
iv
Count
CD107a-PE
Day3 CD107a+ CTLs%
Day5 CD107a+ CTLs %
IFNγhi
IFNγlo

Figure 3

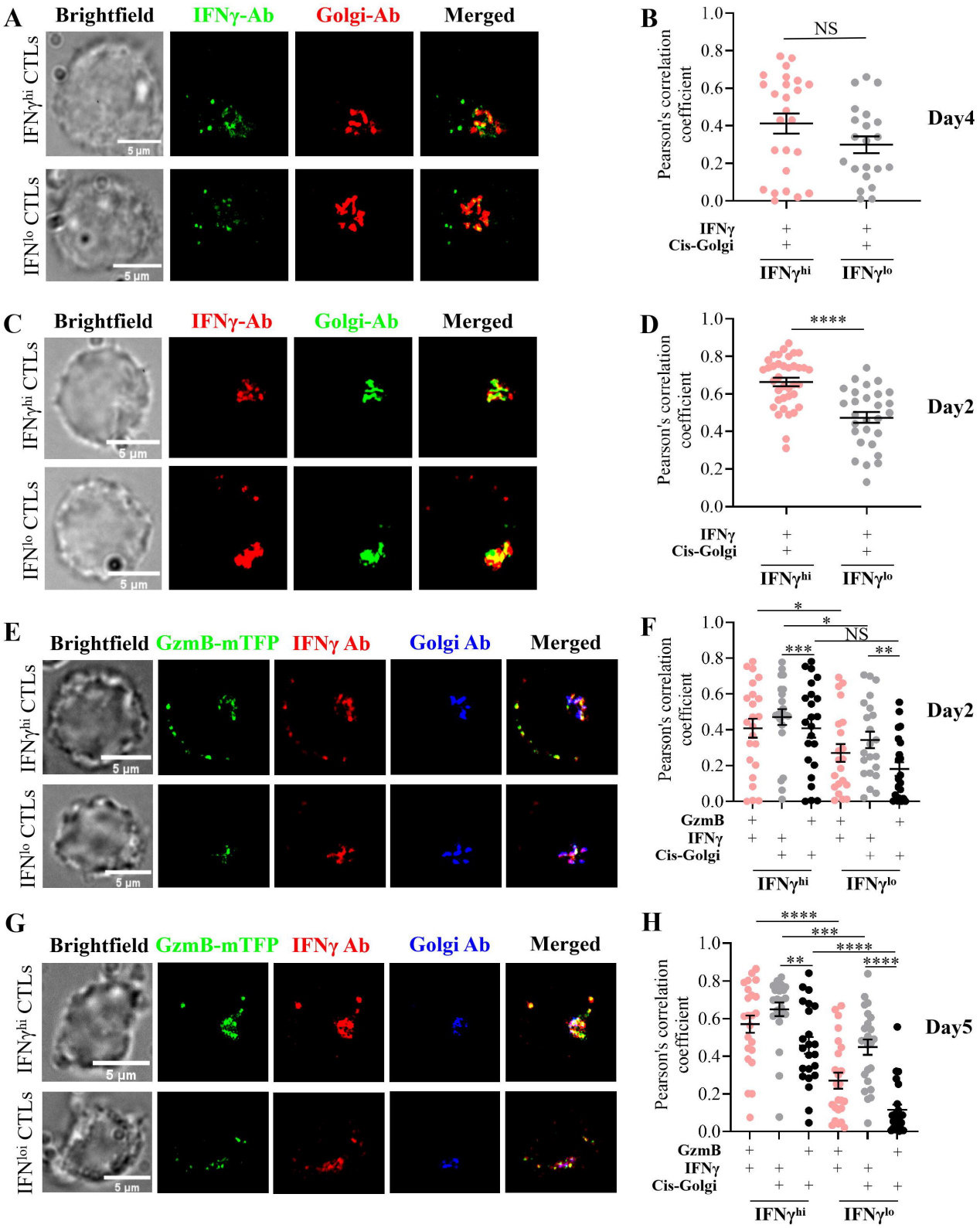
A
Brightfield
IFNγ-Ab
Golgi-Ab
Merged
IFNγhi CTLs
IFNlo CTLs
5 µm
B
Pearson's correlation coefficient
NS
Day4
IFNγ
Cis-Golgi
IFNγhi
IFNγlo
C
D
****
Day2
E
GzmB-mTFP
IFNγ Ab
Golgi Ab
F
*
NS
***
**
GzmB
G
IFNγloi CTLs
H
Day5

Figure 4

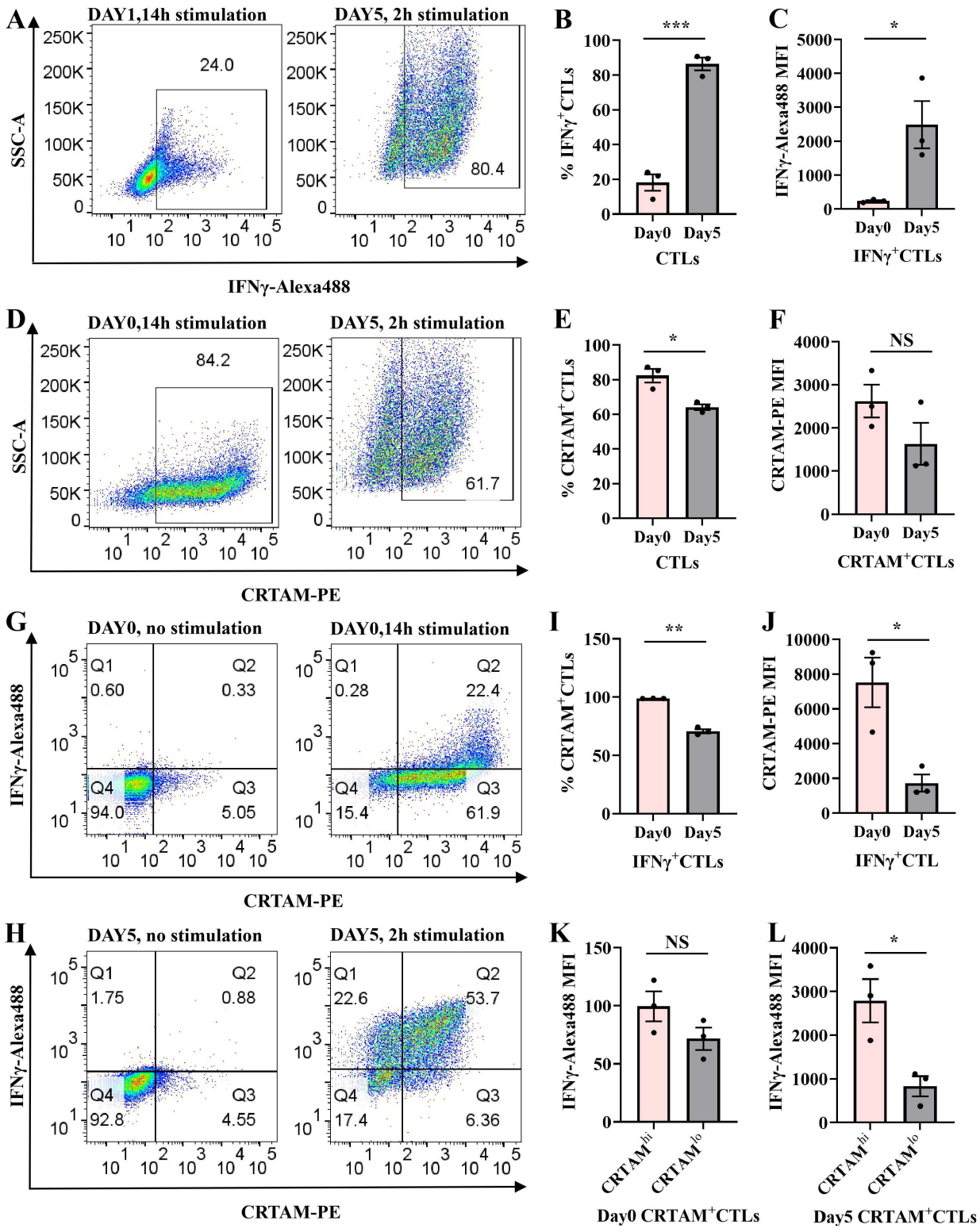
A
DAY1,14h stimulation
DAY5, 2h stimulation
SSC-A
24.0
80.4
IFNγ-Alexa488
B
% IFNγ+CTLs
***
Day0
Day5
CTLs
C
IFNγ-Alexa488 MFI
*
Day0
Day5
IFNγ+CTLs
D
DAY0,14h stimulation
DAY5, 2h stimulation
SSC-A
84.2
61.7
CRTAM-PE
E
% CRTAM+CTLs
*
Day0
Day5
CTLs
F
CRTAM-PE MFI
NS
Day0
Day5
CRTAM+CTLs
G
DAY0, no stimulation
DAY0,14h stimulation
IFNγ-Alexa488
Q1
0.60
Q2
0.33
Q4
94.0
Q3
5.05
Q1
0.28
Q2
22.4
Q4
15.4
Q3
61.9
CRTAM-PE
I
% CRTAM+CTLs
**
Day0
Day5
IFNγ+CTLs
J
CRTAM-PE MFI
*
Day0
Day5
IFNγ+CTL
H
DAY5, no stimulation
DAY5, 2h stimulation
IFNγ-Alexa488
Q1
1.75
Q2
0.88
Q4
92.8
Q3
4.55
Q1
22.6
Q2
53.7
Q4
17.4
Q3
6.36
CRTAM-PE
K
IFNγ-Alexa488 MFI
NS
CRTAMhi
CRTAMlo
Day0 CRTAM+CTLs
L
IFNγ-Alexa488 MFI
*
CRTAMhi
CRTAMlo
Day5 CRTAM+CTLs

Figure 5

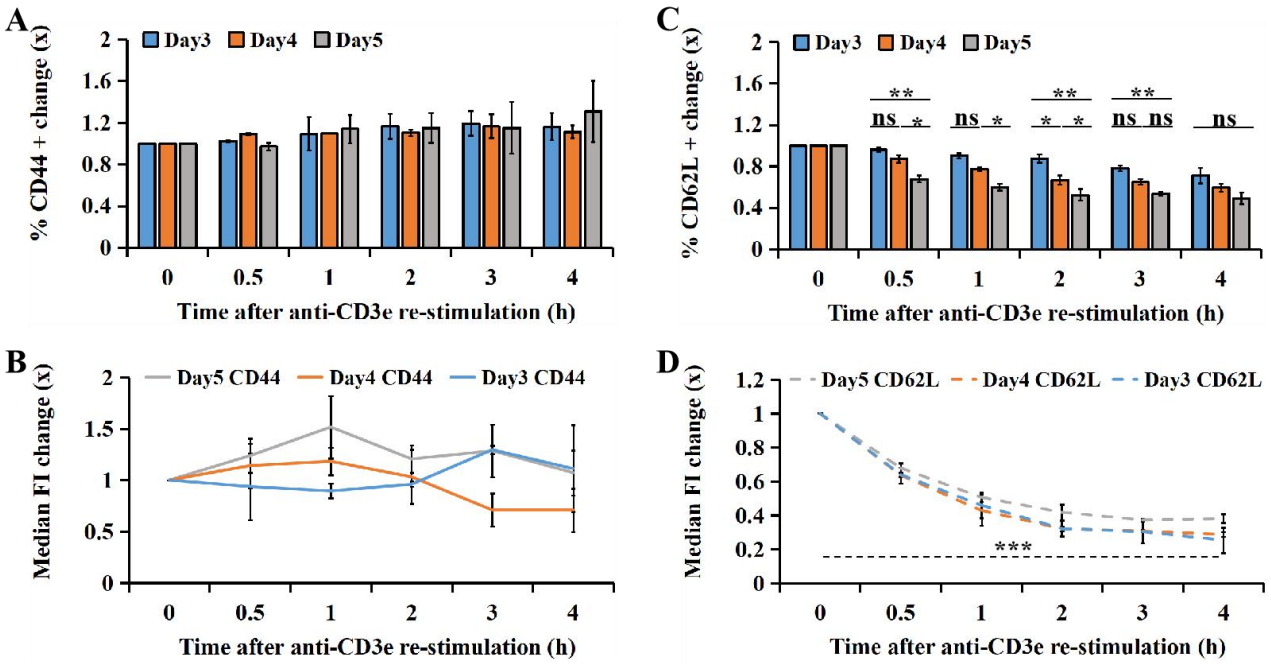

Extended Data Figure 1

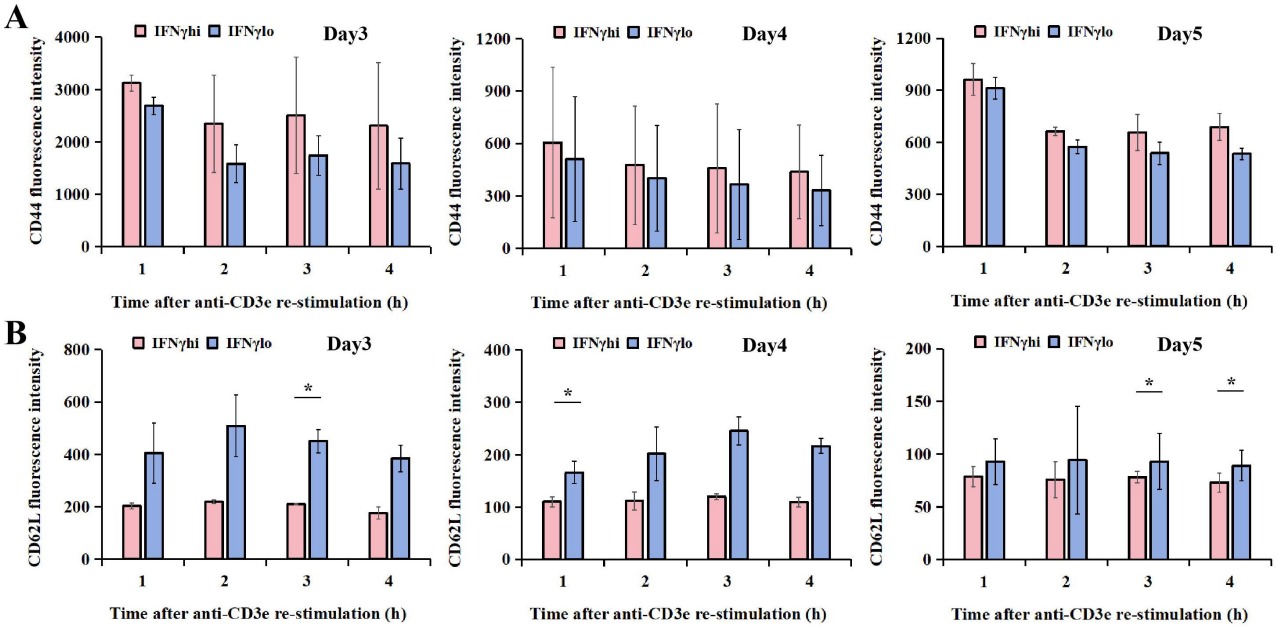

Extended Data Figure 2

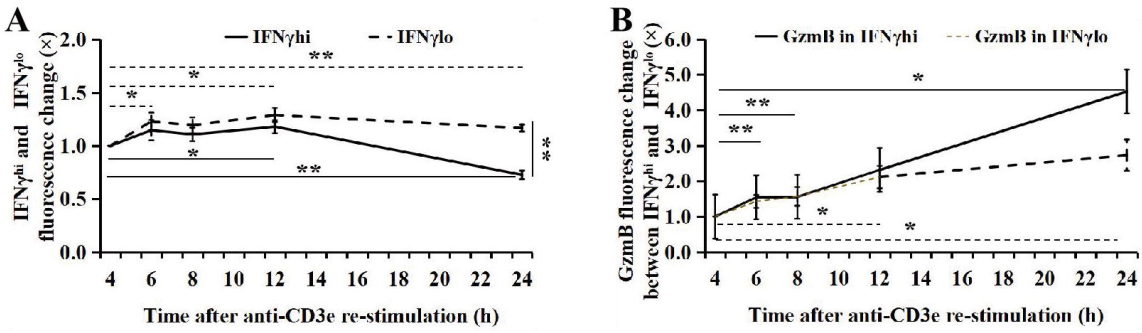

Extended Data Figure 3

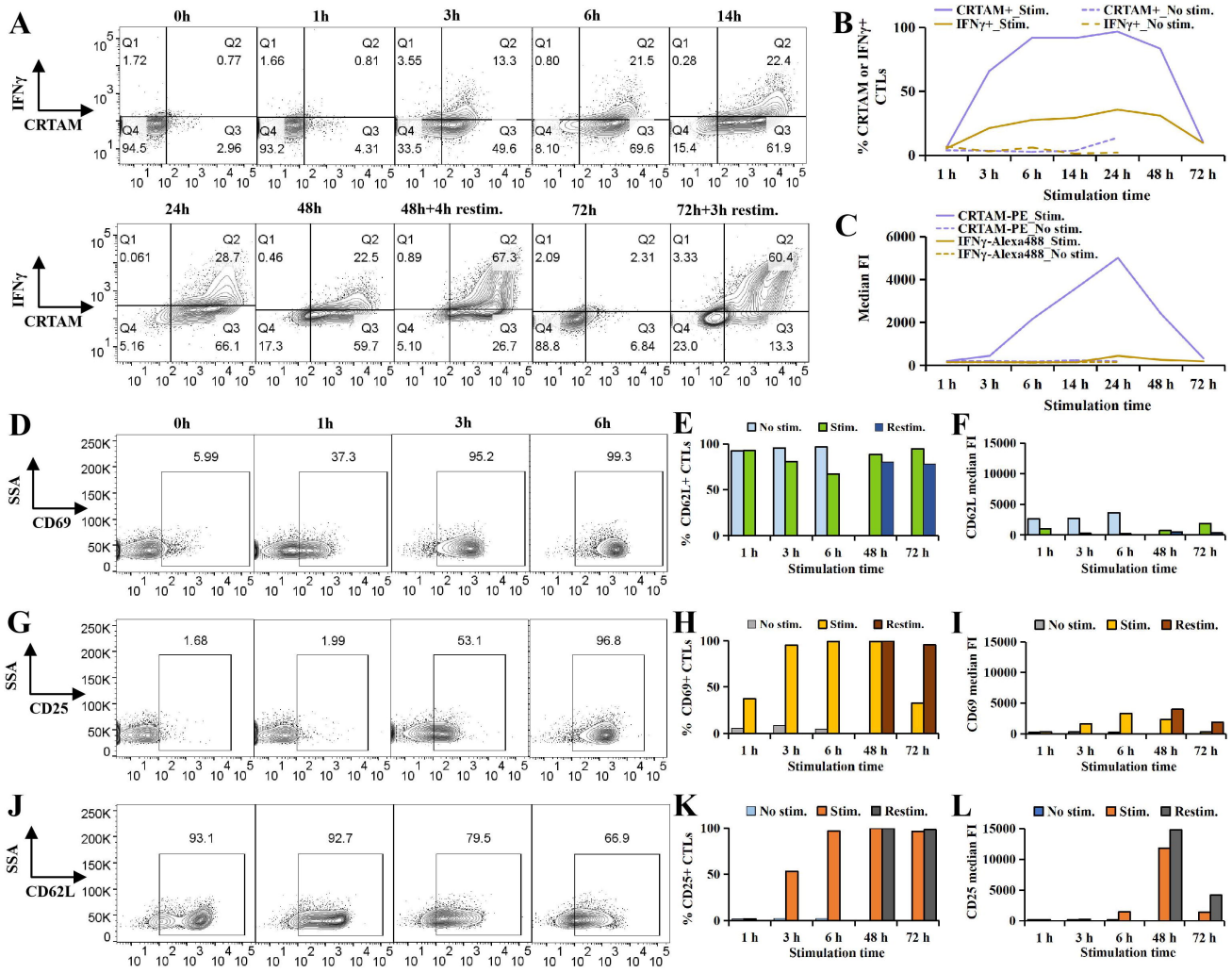

Extended Data Figure 4